ChemComm

COMMUNICATION

View Article Online
View Journal | View Issue



Cite this: *Chem. Commun.*, 2019, 55, 14135

Received 14th October 2019,
Accepted 29th October 2019

DOI: 10.1039/c9cc08054f

rsc.li/chemcomm



# Nanomolar detection of adenosine triphosphate (ATP) using a nanostructured fluorescent chemosensing ensemble†

Ling-Xi Huang,‡[a] Qing Guo,‡[a] Yong Chen,[b] Peter Verwilst,[c] Subin Son,[c] Jia-Bin Wu,[a] Qian-Yong Cao*[a] and Jong Seung Kim*[c]

**We report a novel nanostructured chemosensing ensemble PyNp-C13/UD, obtained by self-assembling uranine dye (UD) and an amphiphilic pyridinium salt PyNp-C13. The ensemble was developed for the fluorescence turn-on sensing of ATP in aqueous solutions and inside living cells. The assembly operates *via* an indicator displacement assay (IDA) method with an ultra-low detection limit of 6.8 nM.**

The development of novel fluorescent chemosensors to selectively detect bioactive anions in the complex matrix of biosystems has attracted increasing attention, due to the relative simplicity and high sensitivity of the fluorescence technique.[1] Among these various anions, sensors for adenosine triphosphate (ATP) have received particular attention, as ATP not only plays a crucial physiological role,[2] but concentrations outside of the normal 1–10 mM range are also observed in several diseases, such as malignant tumours, Alzheimer's disease and Parkinson's disease.[3]

At present, the most widely used approach for designing ATP-sensitive probes is based on the reporter–spacer–receptor (RSR) mechanism, in which the fluorophore signalling unit is covalently attached to an anion receptor.[4] These covalently linked RSR probes often need time-consuming and complicated organic synthesis. A solution to this problem, under the form of so-called chemosensing ensembles, also known as indicator displacement assays (IDAs), was pioneered by the Inouye and Shinkai groups.[5] With this indirect approach, the receptor and indicator dyes form a reversible host/dye complex *via* non-covalent bonds (hydrogen bonds, electrostatic attraction, hydrophilic and hydrophobic interactions, π–π stacking, van der Waals forces or coordination). Analytes compete with the dye and expel the dye from the host, resulting in changes in the optical properties of the dye. The IDA approach shows some advantages over RSRs, such as the ease of synthesis and a wider availability of indicators to allow for the modulation of detection emission wavelengths.

Until now, various host/dye chemosensing ensembles for the recognition of metal ions, anions and biomolecular species have been described.[6] Some examples for the sensing of ATP and other nucleoside polyphosphates have also been reported,[7] and these examples commonly employ macrocyclic receptors, such as cyclophanes, calixarenes, cyclodextrins, cucurbiturils and pillararenes as they show a good binding affinity toward various dyes with remarkable changes in their optical properties.[8] In this work, we employ self-aggregated amphiphilic pyridinium salts as the host, further simplifying the design of the IDA.

Recently, self-assembled nanostructured materials have been attracting much attention in the chemosensor field for their superior characteristics, such as high sensitivity and excellent biocompatibility.[9] While some fluorescent amphiphile-based nanoaggregates for the recognition of ATP and other related triphosphate nucleotides have been developed, the design usually consists of an amphiphilic RSR design.[10] Here, we report a nanostructured chemosensing ensemble **PyNp-C13/UD** (see Scheme 1) based on the indicator displacement assay (IDA) method.

The amphiphilic pyridinium-based receptor **PyNp-C13** was designed based on the following rationale: (1) the multiple pyridinium and amide donors can efficiently participate in anion binding *via* hydrogen bonding and/or electrostatic interactions, (2) the long dodecylcetyl chain enables self-assembly in aqueous solutions due to hydrophobic interactions, and (3) pyridinium is a useful fluorescence quenching unit.[11] Using the commercially available uranine dye (**UD**) as the fluorescent indicator, we found that **PyNp-C13** binds well with the anionic dye and results in a self-assembled nanostructure (**PyNp-C13/UD**) in pure aqueous solutions. As a result of PET (photoinduced electron transfer) quenching from the pyridinium salt to **UD**, the fluorescence of the ensemble was very weak, but competition with ATP liberated the fluorescent dye resulting in a large increase in fluorescence.

The synthesis of the amphiphilic receptor **PyNp-C13**, following a literature procedure, is described in detail in the ESI† and the

[a] *Department of Chemistry, Nanchang University, Nanchang 330031, P. R. China. E-mail: cqyong@ncu.edu.cn; Fax: +86 791-83969386*
[b] *Institute for Advanced Study, Nanchang University, Nanchang 330031, China*
[c] *Department of Chemistry, Korea University, Seoul 02841, Korea. E-mail: jongskim@korea.ac.kr*

† Electronic supplementary information (ESI) available: Experimental details, NMR spectra and additional spectroscopic data. See DOI: 10.1039/c9cc08054f

‡ These authors contributed equally.

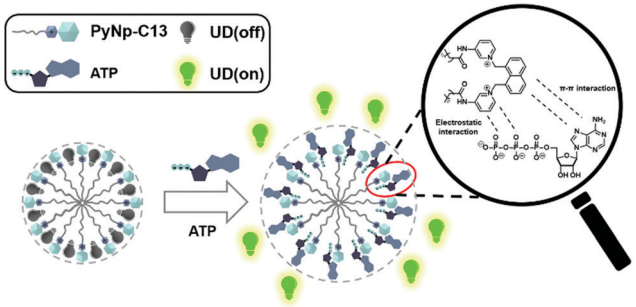


Scheme 1 The structure of **PyNp-C13** and the IDA-based ATP sensing mechanism.

compound, alongside a short-chain analogue (**PyNp-C1**), was fully characterized by $^{1}H/^{13}C$ NMR and HR-MS.

We first studied the interactions between **UD** and **PyNp-C13**, using absorbance and fluorescence spectroscopy. The successive addition of **PyNp-C13** to **UD** (6 μM) in a HEPES (1.0 mM, pH = 7.4) buffer solution resulted in a gradual decrease in the absorption of **UD** at 490 nm concomitant with the formation of a new peak at 515 nm (Fig. 1a and Fig. S1, ESI†), with a characteristic isosbestic point at 502 nm, indicating the formation of only one species of host–guest inclusion complex. The addition of **PyNp-C13** also resulted in a drastic change in **UD** fluorescence at 515 nm (Fig. 1b and Fig. S2, ESI†), with a nearly complete fluorescence quenching (99.5%) upon the addition of 12 μM **PyNp-C13**. The emission quantum yield (QY) and emission lifetime of **UD** and **PyNp-C13/UD** were also investigated, with the QYs of 31.7% and 0.3%, and emission lifetime values of 4.5 ns and 3.2 ns (Fig. S3, ESI†), respectively. Clearly, **PyNp-C13** and **UD** can form a stable complex in aqueous solutions, which may be attributed to the electrostatic interaction and/or hydrogen bonding between the cationic **PyNP-C13** host with the anionic UD. The Benesi–Hildebrand analysis of the emission data gave a 2 : 1 stoichiometry complexation for the **PyNp-C13/UD** ensemble, with a binding constant of $3.42 \times 10^{10}$ $M^{-2}$.

The formation of the **PyNp-C13/UD** ensemble was further confirmed by a Tyndall experiment, dynamic light scattering (DLS) and transmission electron microscopy (TEM). It was observed that the free receptor **PyNp-C13** and **UD** are soluble at the tested concentration without a Tyndall phenomenon, however the **PyNp-C13/UD** ensemble exhibits a clear Tyndall effect (Fig. S4, ESI†). Clearly, the **PyNp-C13/UD** ensemble

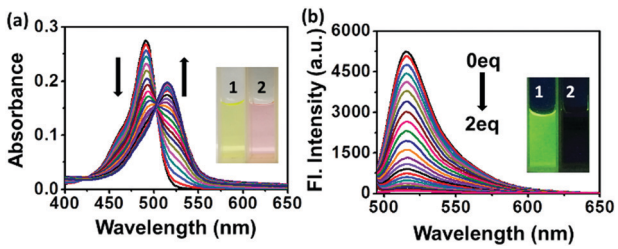


Fig. 1 The UV-vis (a) and fluorescence (b) spectra of **UD** (6 μM, $\lambda_{ex}$ = 490 nm) upon the addition of various amounts of **PyNp-C13** in HEPES (10 mM, pH = 7.4) buffer solution. The inset shows the colour change of **UD** after the addition of 2.0 equivalents of **PyNp-C13** in ambient light and with excitation at 365 nm using a hand-held UV light.

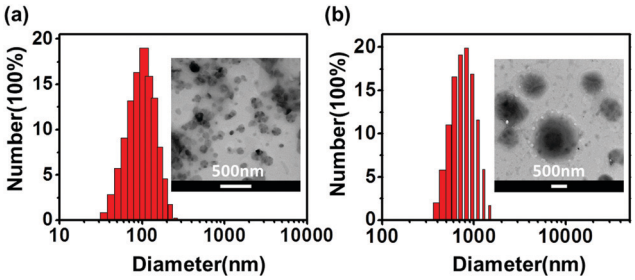


Fig. 2 The size distribution of the **PyNp-C13/UD** assembly before (a) and after (b) addition of 8 equivalents of ATP in aqueous solution. The insets show their corresponding TEM images.

self-assembled into micelle-like nano-structured aggregates. A DLS experiment indicated that the **PyNp-C13/UD** nanoassembly shows an average hydrated diameter of 115 nm in aqueous solutions, while the TEM data shows sphere-like aggregates with a diameter of 60–90 nm in the solid state (Fig. 2).

We further tested the potential of the **PyNp-C13/UD** ensemble (12 μM/6 μM) in HEPES buffer as an IDA system for polyphosphate anions such as ATP. Upon the addition of ATP, the absorbance of the **PyNp-C13/UD** ensemble at 515 nm gradually blue shifted to 490 nm, as the solution colour recovered from pink to yellow (Fig. S5, ESI†). Additionally, a broad absorbance at 530–600 nm became apparent during the titration as well, which can be attributed to the formation of larger nanoaggregates.

The emission titration results also confirm that the addition of ATP can recover the **UD** green emission (Fig. 3a). The gradually increasing emission process is saturated with the addition of about 8 equivalents ATP, and the fluorescence recovery rate reaches 68.9%. The binding constant between **PyNp-C13/UD** and ATP was

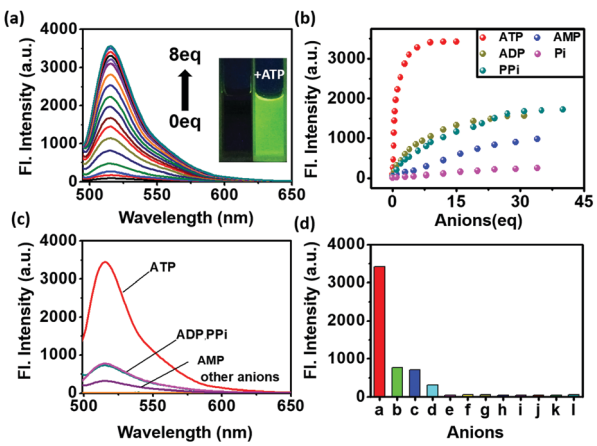


Fig. 3 (a) Fluorescence changes of **PyNp-C13/UD** (12 μM/6 μM, $\lambda_{ex}$ = 490 nm) upon the addition of various amounts of ATP in a HEPES solution (10 mM, pH = 7.4); the inset shows the fluorescence of **PyNp-C13/UD** before and after the addition of 8.0 equivalents of ATP using a hand-held UV light. (b) Fluorescence intensities of **PyNp-C13/UD** at 515 nm *versus* the number of equivalents of several phosphate anions. (c) Fluorescence spectra of **PyNp-C13/UD** (12 μM/6 μM) before and after the addition of 4.0 equivalents of several phosphate anions in a HEPES buffered solution. (d) Relative fluorescence histogram chart of **PyNp-C13/UD** at 515 nm upon the addition of 8 equivalents of various anions (a: ATP, b: ADP, c: PPi, d: AMP, e: Pi, f: $AcO^-$, g: $F^-$, h: $Cl^-$, i: $Br^-$, j: $I^-$, k: $CO_3^{2-}$, l: $SO_4^{2-}$).

 

determined to be $1.0 \times 10^{11}$ $M^{-2}$ according to the emission titration data (Fig. S6, ESI†), with a 2 : 1 stoichiometry. In addition, the detection limit of **PyNp-C13/UD** toward ATP was calculated to be 6.8 nM, indicating that this system can efficiently and quantitatively detect ATP at very low concentrations.

Subsequently, we repeated similar experiments in the presence of other phosphate anions, including ADP and AMP, inorganic phosphates PPi and Pi, and other biologically relevant anions ($AcO^-$, $F^-$, $Cl^-$, $Br^-$, $I^-$, $CO_3^{2-}$, and $SO_4^{2-}$). A moderate to weak response toward PPi, ADP and AMP, with a partial recovery of the absorption and emission spectra of **UD**, was observed (Fig. S7–S9, ESI†). The binding constants and detection limits of **PyNp-C13/UD** toward these anions were also calculated and listed in Table S1 (ESI†). Interestingly, the complexation ratio between these anions and **PyNp-C13/UD** follows a 1 : 1 stoichiometry. As can be seen, the binding affinity of **PyNp-C13/UD** toward these polyphosphates follows the order of ATP ≫ ADP ≈ PPi ≫ AMP. Thus, the **PyNp-C13/UD** ensemble is a useful sensor for fluorescence detection of ATP in neutral aqueous solutions. The selectivity for ATP over ADP and AMP is important, because the ATP/ADP ratio in cells is an important modulator for a variety of cellular events.[12]

The high displacement affinity of **PyNp-C13/UD** toward ATP over ADP, PPi and other anions can also be confirmed by DLS experiments (Fig. S10, ESI†). The mean size of the **PyNp-C13/UD** nanoaggregation ensemble shows a large increase from 106 nm to 1100 nm after displacement by ATP anions in aqueous solutions. Only a moderate size increase was observed for ADP (290 nm) and PPi (250 nm), while other ions did not induce significant changes. These results are further confirmed by the TEM data, in which the spherical aggregates of **PyNp-C13/UD** changed from a diameter of 60–90 nm to 500–900 nm upon the addition of ATP (Fig. 2).

In addition, we also investigated the sensing ability of the control compound **PyNp-C1**, which lacks the long hydrophobic alkyl tail. **PyNp-C1** shows weaker binding ability toward **UD** anions compared to **PyNp-C13** ($3.42 \times 10^{10}$ $M^{-2}$ *vs.* $8.4 \times 10^{9}$ $M^{-2}$, Fig. S11, ESI†), with a lower fluorescence quenching ratio (99.5% *vs.* 87.2%). In addition, the formed **PyNp-C1/UD** assembly exhibits a much lower recognition ability toward ATP (17.8%, Fig. S12, ESI†), thus confirming the benefit of the self-assembled nano-sized micelle architecture.

The larger UV-vis absorption and fluorescence changes indicate strong interaction between **PyNp-C13** and **ATP/UD** anions, which is further confirmed by $^1$H NMR titrations in DMSO-$d_6$/$D_2O$ (8 : 2, v/v). As shown in Fig. S13 (ESI†), the pyridinium protons $H_a$, $H_b$ and $H_c$ and methylene protons $H_d$ of **PyNp-C13** locate at 9.37, 8.63, 8.36 and 6.48 ppm, respectively. Upon the addition of **ATP** or **UD** anions, these protons display an obvious down-field shift. Compared with **PyNp-C13/UD** ($\Delta\delta$ = 0.07, 0.07, 0.13 and 0.09 ppm, respectively), **PyNp-C13/ATP** ($\Delta\delta$ = 0.21, 0.14, 0.19 and 0.14 ppm, respectively) shows larger changes in chemical shift, which is consistent with stronger interactions for ATP relative to **UD**.

In order to achieve the sensing ability of ATP in cells, the influence of pH on the fluorescence response of **PyNp-C13/UD** was investigated (Fig. 4a). It was found that **PyNp-C13/UD** showed only a weak response in highly acid solutions (pH < 5) as well as under alkaline conditions (pH > 11). However, a remarkable fluorescence enhancement was observed in the pH range of 6–10, indicating that **PyNp-C13/UD** can detect ATP under physiological conditions. The influence of other anions on the sensitivity towards ATP was also studied. As shown in Fig. S14 (ESI†), virtually no interference was observed.

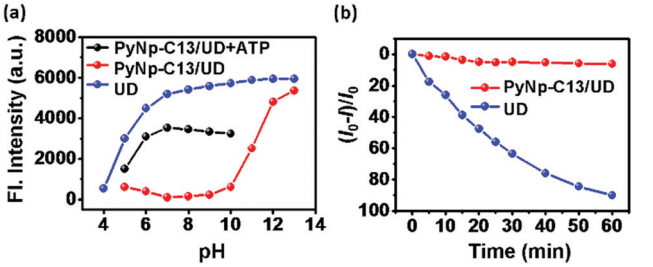


Fig. 4 (a) Fluorescence intensity at 515 nm of **UD** (6 μM), **PyNp-C13/UD** (12 μM/6 μM) and **PyNp-C13/UD** + ATP (10 equivalents) at different pH values. (b) Fluorescence stability of **UD** (6 μM) and **PyNp-C13/UD** (12 μM/6 μM) with increasing exposure time of a xenon lamp (300 W). The fluorescence intensity of **PyNp-C13/UD** was recorded as fluorescence intensity loss (%) in the presence of ATP (60 μM) at pH 7.4.

A photo-stability experiment of **PyNp-C13/UD** (12 μM/6 μM) in a HEPES buffered solution was carried out, where the ensemble was first exposed to a 300 W xenon lamp, then ATP was added and the fluorescence intensity at 515 nm was recorded. As shown in Fig. 4b, **PyNp-C13/UD** exhibits high photo-stability, with the fluorescence intensity loss <5% under continuous irradiation for 1 h. By contrast, a solution of **UD** alone results in almost 90% fluorescence bleaching. This difference may be attributed to a shielding effect by **PyNp-C13**, which can prevent interactions between **UD** molecules and decrease the probability of photochemical reactions between excited **UD** and reactive species such as water and oxygen.[10c] In addition, **UD** in the **PyNp-C13/UD** ensemble is maintained in a dark emission state, further causing resistance to photo-oxidation and photo-bleaching.

Because of the good selectivity and high affinity of **PyNp-C13/UD** toward ATP, we next applied this probe to image the ATP levels in living cells. First, the cytotoxicity of **PyNp-C13/UD** (2 : 1 ratio) was tested in murine liver cancer cells (Hepa1-6). With the concentration of the nanostructure ranging from 0 to 40 μM, more than 80% cell survival was observed after incubation for 24 hours, demonstrating the low toxicity of this assembly (Fig. S15, ESI†). Having confirmed the low cytotoxicity of the nanostructured IDA sensor, the ensemble's potential for ATP sensing was tested in living cells. Fig. 5 shows the CLSM images of **PyNp-C13/UD** (12 μM/6 μM) incubated with living Hepa1-6 cells. To control the cellular ATP levels, three sets of cells were selected: a control sample, cells treated with sodium azide (5 mM), and cells treated with $Ca^{2+}$ (5 mM). Sodium azide was used as a mitochondrial poison, uncoupling the mitochondrial oxidative phosphorylation (OXPHOS) to inhibit mitochondrial ATPase, and thus induce an abrupt decrease of ATP concentration,[13] while $Ca^{2+}$ activates dehydrogenase in mitochondria, thereby raising the concentration of NADH and ATP.[14] As shown in Fig. 5, the addition of sodium azide resulted in a decrease of the

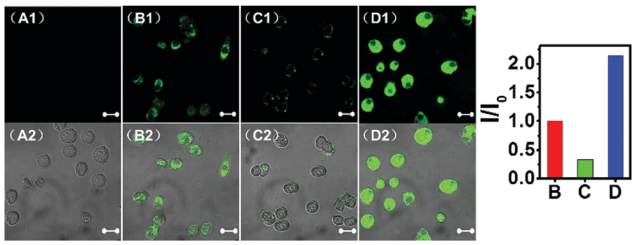


Fig. 5 Fluorescent monitoring of the ATP level in living Hepa1-6 cells. Left: CLSM images of Hepa1-6 cells alone (A1 and A2); **PyNp-C13/UD** (12 μM/6 μM) was incubated with Hepa1-6 cells for 2 hours (B1 and B2); Hepa1-6 cells were first treated with 10 mM $NaN_3$ and then incubated with **PyNp-C13/UD** for 2 hours. (C1 and C2); Hepa1-6 cells were first treated with 5 mM $Ca^{2+}$ and then incubated with **PyNp-C13/UD** for 2 hours (D1 and D2). Scale bar, 20 μm. Right: Relative fluorescence intensity of B, C, and D.

fluorescence intensity up to 33.3%, compared to the control group, while treatment of cells with $Ca^{2+}$ resulted in a 214.3% increase in fluorescence. Thus, **PyNp-C13/UD** demonstrated the capability for monitoring ATP levels in living cells.

To assess the applicability of **PyNp-C13/UD** toward ATP in more complex environments, fluorescence imaging experiments were performed in living *C. elegans* (Fig. S16, ESI†). Nematodes were pre-treated with exogenous ATP (100 μM) at 20 °C for 4 h, and then incubated with **PyNp-C13/UD** (40 μM/20 μM) for a further 3 h. Strong green fluorescence was observed in the entire nematode body. By contrast, nematodes treated with only **PyNp-C13/UD** (Fig. S20B, ESI†) exhibited negligible fluorescence. These results indicate the feasibility and reliability of the present assay for ATP detection under practical biological conditions.

In conclusion, we successfully applied a cationic pyridinium amphiphile **PyNp-C13** to the recognition of ATP using the IDA method. This receptor can self-assemble with **UD** to form non-fluorescent **PyNp-C13/UD** nanoaggregates *via* multiple electrostatic interactions, hydrogen bonding and hydrophobic interactions in aqueous solutions. This **PyNp-C13/UD** ensemble demonstrated a high sensitivity and selectivity toward ATP for the successful displacement of the fluorescent indicator **UD** from the complex, with a fluorescence turn-on response. In addition, **PyNp-C13/UD** demonstrates a low cytotoxicity and a high cell permeability and is suitable for imaging ATP levels in living cells. This system shows advantages over previously reported methods, such as easy synthesis, simple operation, high photo-stability and the detection of ATP levels *in vitro* in pure aqueous solutions. The expansion of the current design toward other nucleoside phosphates and IDAs with different indicators is currently in progress.

This work was supported by the National Natural Science Foundation of China (No. 21762028, QYC), the Interdisciplinary Innovation Fund of Nanchang University (Project No. 2019-9166-27060003, QYC), and a CRI project (No. 2018R1A3B1052702, JSK) of the National Research Foundation of Korea (NRF).

## Conflicts of interest

There are no conflicts to declare.

## Notes and references

1 (*a*) N. Busschaert, C. Caltagirone, R. W. Van and P. A. Gale, *Chem. Rev.*, 2015, **115**, 8038–8155; (*b*) T. D. Ashton, K. A. Jolliffe and F. M. Pfeffer, *Chem. Soc. Rev.*, 2015, **44**, 4547–4595; (*c*) P. A. Gale and C. Caltagirone, *Coord. Chem. Rev.*, 2018, **354**, 2–27; (*d*) J. Wu, W. Liu, J. Ge, H. Zhang and P. Wang, *Chem. Soc. Rev.*, 2011, **40**, 3483–3495.
2 (*a*) J. R. Knowles, *Annu. Rev. Biochem.*, 1980, **49**, 877–919; (*b*) A. V. Gourine, E. Llaudet, N. Dale and K. M. Spyer, *Nature*, 2005, **436**, 108–111.
3 G. Burnstock, *Trends Pharmacol. Sci.*, 2006, **27**, 166–176.
4 (*a*) A. E. Hargrove, S. Nieto, T. Zhang, J. L. Sessler and E. V. Anslyn, *Chem. Rev.*, 2011, **111**, 6603–6782; (*b*) S. Lee, K. K. Yuen, K. A. Jolliffe and J. Yoon, *Chem. Soc. Rev.*, 2015, **44**, 1749–1762; (*c*) Q. Zhao, Z. Zhang and Y. Tang, *Chem. Commun.*, 2017, **53**, 9414–9417; (*d*) L. Wang, L. Yuan, X. Zeng, J. Peng, Y. Ni, J. C. Er, W. Xu, B. K. Agrawalla, D. Su, B. Kim and Y. T. Chang, *Angew. Chem., Int. Ed.*, 2016, **55**, 1773–1776; (*e*) D. Maity, M. Li, M. Ehlers and C. Schmuck, *Chem. Commun.*, 2017, **53**, 208–211; (*f*) H.-B. Cheng, Z. W. Sun, N. Kwon, R. Wang, Y. Cui, C. O. Park and J. Yoon, *Chem. – Eur. J.*, 2019, **25**, 3501–3504; (*g*) G. Jiang, W. Zhu, Q. Chen, A. Shi, Y. Wu, G. Zhang, X. Li, Y. Li, X. Fan and J. Wang, *Analyst*, 2017, **142**, 4388–4392.
5 (*a*) B. T. Nguyen and E. V. Anslyn, *Coord. Chem. Rev.*, 2006, **250**, 3118–3127; (*b*) J. Wu, B. Kwon, W. Liu, E. V. Anslyn, P. Wang and J. S. Kim, *Chem. Rev.*, 2015, **115**, 7893–7943.
6 (*a*) Y. Liu, L. Perez, M. Mettry, C. J. Easley, R. J. Hooley and W. Zhong, *J. Am. Chem. Soc.*, 2016, **138**, 10746–10749; (*b*) M. A. Beatty, J. Borges-Gonzalez, N. J. Sinclar, A. T. Pye and F. Hof, *J. Am. Chem. Soc.*, 2018, **140**, 3500–3504; (*c*) A. Norouzy, Z. Azizi and W. M. Nau, *Angew. Chem., Int. Ed.*, 2015, **54**, 792–795; (*d*) V. E. Zwicker, B. L. Oliveira, J. H. Yeo, S. T. Fraser, G. J. L. Bernardes, E. J. New and K. A. Jolliffe, *Angew. Chem., Int. Ed.*, 2019, **58**, 3087–3091.
7 (*a*) J. Deng, K. Wang, M. Wang and P. Yu, *J. Am. Chem. Soc.*, 2017, **139**, 5877–5882; (*b*) P. P. Neelakandan, M. Hariharan and D. Ramaiah, *J. Am. Chem. Soc.*, 2006, **128**, 11334–11335; (*c*) J. Gao, J. Li, W. C. Geng, F. Y. Chen, X. Duan, Z. Zheng, D. Ding and D. S. Guo, *J. Am. Chem. Soc.*, 2018, **140**, 4945–4953; (*d*) M. Bojtár, J. Kozmaa, Z. Szakács, D. Hesszc, M. Kubinyi and I. Bitter, *Sens. Actuators, B*, 2017, **248**, 305–310.
8 R. Kumar, A. Sharma, H. Singh, P. Suating, H. S. Kim, K. Sunwoo, I. Shim, B. C. Gibb and J. S. Kim, *Chem. Rev.*, 2019, **119**, 9657–9721.
9 (*a*) X. Ma and Y. Zhao, *Chem. Rev.*, 2015, **115**, 7794–7839; (*b*) R. Klajn, J. F. Stoddart and B. A. Grzybowski, *Chem. Soc. Rev.*, 2010, **39**, 2203–2237; (*c*) G. Yu, K. Jie and F. Huang, *Chem. Rev.*, 2015, **115**, 7240–7303; (*d*) C. T. Li, Y. L. Xu, J. G. Yang, Y. Chen, H. S. Kim, Q. Y. Cao and J. S. Kim, *Sens. Actuators, B*, 2017, **251**, 617–623; (*e*) Q. Guo, Y. Zhang, Z. H. Lin, Q. Y. Cao and Y. Chen, *Dyes Pigm.*, 2020, **172**, 107872.
10 (*a*) H. Tao, L. He, G. Cheng and Q.-Y. Cao, *Dyes Pigm.*, 2019, **166**, 233–238; (*b*) J. H. Zhu, C. Yu, Y. Chen, J. Shin, Q.-Y. Cao and J. S. Kim, *Chem. Commun.*, 2017, **53**, 4342–4345; (*c*) X. Li, X. Guo, L. Cao, Z. Xun, S. Wang, S. Li, Y. Li and G. Yang, *Angew. Chem., Int. Ed.*, 2014, **53**, 7809–7813.
11 L. Cheng, H. Zhang, Y. Dong, Y. Zhao, Y. Yu and L. Cao, *Chem. Commun.*, 2019, **55**, 2372–2375.
12 S. H. Hewitt, J. Parris, R. Mailhot and S. J. Butler, *Chem. Commun.*, 2017, **53**, 12626–12629.
13 M. W. Bowler, M. G. Montgomery, A. G. Leslie and J. E. Walker, *Proc. Natl. Acad. Sci. U. S. A.*, 2006, **103**, 8646–8649.
14 E. J. Griffiths and G. A. Rutter, *Biochim. Biophys. Acta, Bioenerg.*, 2009, **1787**, 1324–1333.

 